

From Hermitian critical to non-Hermitian point-gapped phases

Carlos Ortega-Taberner  and Maria Hermanns 

Department of Physics, Stockholm University, AlbaNova University Center, 106 91 Stockholm, Sweden and Nordita, KTH Royal Institute of Technology and Stockholm University, 106 91 Stockholm, Sweden



(Received 16 January 2023; revised 1 May 2023; accepted 2 May 2023; published 6 June 2023)

Recent years have seen a growing interest in topological phases beyond the standard paradigm of gapped isolated systems. One recent direction is to explore topological features in non-Hermitian systems that are commonly used as effective descriptions of open systems. Another direction explores the fate of topology at critical points, where the bulk gap collapses. One interesting observation is that both systems, though very different, share certain topological features. For instance, both systems can host half-integer quantized winding numbers and have very similar entanglement spectra. Here we make this similarity explicit by showing the equivalence of topological invariants in critical systems with non-Hermitian point-gap phases, in the presence of sublattice symmetry. Also, the corresponding entanglement spectra show the same topological features. This correspondence may carry over to other features and even be helpful to deepen our understanding of non-Hermitian systems using our knowledge of critical systems and vice versa.

DOI: [10.1103/PhysRevB.107.235112](https://doi.org/10.1103/PhysRevB.107.235112)

I. INTRODUCTION

In recent years non-Hermitian systems have attracted a great deal of attention in the condensed-matter community due to the unique phenomena that they can exhibit. In the field of symmetry protected topological phases, non-Hermitian systems harbor a particularly rich variety of phases, as the non-Hermiticity enhances the ten Hermitian topological classes [1–3] into 38 [4–7]. This enhancement originates in having effectively more symmetries available, as conjugation and transposition are not equivalent any longer. Furthermore, non-Hermiticity may lead to new physics without a Hermitian equivalent: So-called point-gap phases and exceptional points [8,9] lead to new physics with no Hermitian equivalent, like the skin effect [5,8,10–13].

For non-Hermitian systems, we need to distinguish between line-gapped and point-gapped systems. For the former, it is possible to draw a line in the complex plane which separates the different bands. On the other hand, a phase is said to be point gapped at E_0 if it has a nonzero energy vorticity for this point, i.e., the complex energy bands wind around E_0 . While the topology of line-gapped systems can be understood from their connection to Hermitian and anti-Hermitian Hamiltonians [6], point-gapped systems have features that are thought to be intrinsically non-Hermitian. In this paper we focus on these systems and show how some of their features are inherited from related Hermitian critical models.

The topic of topological phenomena in critical systems has recently been revisited [14–18]. Topology is a global (non-local) property of the system and it was previously thought that the divergent correlation length of critical systems always rendered the system topologically trivial. However, it has been shown recently that this is not the case [14]. Critical systems can harbor topologically protected zero-energy edge states that are protected by a topological invariant and do not hybridize with the bulk. The topological phases in these systems have been characterized by invariants that are quantized to half-integers [15].

The latter is also true for some non-Hermitian systems. For example, systems in the topological class AI (with a sublattice symmetry S that commutes with time reversal) are characterized by two winding numbers which can take half-integer values when the system has a point gap [5,19–21]. This similarity in the topology of Hermitian critical and non-Hermitian systems has been pointed out in the literature before [22], but it has not yet been explored in depth. In this paper we aim to relate the bulk topological features of critical Hermitian systems and point-gapped non-Hermitian systems. We will introduce two different methods of generalizing a Hermitian critical Hamiltonian to a non-Hermitian one, showing that the resulting model always is in a point-gap phase. We also analyze how bulk topological features evolve with the non-Hermiticity, in particular the topological invariants and the so-called entanglement occupancy spectrum (EOS) [23–25]. While the two generalizations considered here are somewhat limited, the second includes two of the most used non-Hermitian models, the Hatano-Nelson model and the Su-Schrieffer-Heeger (SSH) chain with unbalanced hopping.

In Hermitian systems the EOS, computed for periodic boundary conditions, provides the same topological information as the surface energy spectrum [26,27], and it has been connected to topological invariants such as the polarization

Published by the American Physical Society under the terms of the Creative Commons Attribution 4.0 International license. Further distribution of this work must maintain attribution to the author(s) and the published article's title, journal citation, and DOI. Funded by Bibsam.

[28] and the winding number [29]. For non-Hermitian point-gapped systems the bulk-boundary correspondence is broken due to the skin effect. Thus one cannot use the surface spectrum to study bulk topology (and vice versa). In this case, the EOS becomes more interesting, as it can be computed for periodic boundary conditions and can be related to bulk invariants [30,31]. We show that the topological features of the EOS of non-Hermitian point-gap phases are dictated by the related Hermitian critical one, thus providing a physical interpretation for the former. More generally, connecting Hermitian critical and non-Hermitian point-gap systems would allow one to compute objects for non-Hermitian models using Hermitian physics, as well as use the more developed topological classification for non-Hermitian systems to address questions regarding critical Hermitian systems.

The paper is organized as follows. In Sec. II we cover some necessary background material. In Sec. III we consider a very simple non-Hermitian generalization to elucidate the main ideas. A more complex generalization is shown in Sec. IV, where the non-Hermiticity is introduced by making the momenta complex. The entanglement occupancy spectrum is discussed in Sec. V. Some explicit examples are covered in Appendix A.

II. BACKGROUND

Throughout the paper, we restrict the discussion to a general two-band model given by the Hamiltonian

$$\begin{aligned} H(k) &= \mathbf{h}(k) \cdot \boldsymbol{\sigma} = h_x(k)\sigma_x + h_y(k)\sigma_y \\ &= \begin{pmatrix} 0 & f_1(k) \\ f_2(k) & 0 \end{pmatrix}, \end{aligned} \quad (1)$$

where we set h_z to zero because of sublattice symmetry. Both ways of describing the Hamiltonian will prove useful in the following. Note that for non-Hermitian models, $f_2(k) \neq f_1^*(k)$, while in the Hermitian case we suppress the index and use $f(k) \equiv f_1(k) = f_2^*(k)$. The right eigenstates of such two-band Hamiltonians are in general given by

$$v_{\pm}^R(k) = \frac{1}{\sqrt{2}}[\pm\sqrt{f_1(k)/f_2(k)}, 1], \quad (2)$$

with energies $\pm\sqrt{f_1(k)f_2(k)}$. The corresponding left ones are

$$v_{\pm}^L(k) = \frac{1}{\sqrt{2}}[\pm\sqrt{f_2(k)/f_1(k)}, 1]. \quad (3)$$

For Hermitian two-band models, the winding number [3] can be written as

$$\nu = \frac{1}{2\pi} \int_0^{2\pi} dk \partial_k \arg[h_x(k) - ih_y(k)] \quad (4)$$

or alternatively as

$$\nu = \frac{1}{2\pi} \int_0^{2\pi} dk \frac{[\partial_k h_x(k)]h_y(k) - h_x(k)\partial_k h_y(k)}{h_x(k)^2 + h_y(k)^2}. \quad (5)$$

For non-Hermitian models both expressions are no longer equal. The second expression (5) is usually employed to compute the winding number [5,6,19]. While the Hamiltonian (1) is of course restrictive, it nevertheless covers two of the most studied non-Hermitian models, the Hatano-Nelson

model [32–34] and the non-Hermitian extension to the SSH model [35].

A. Topological invariants for critical systems

Topological invariants are usually considered meaningful only in gapped systems. This raises the question if and how topological features survive the presence of gapless modes, e.g., by coupling to a gapless environment [36] or by driving to a phase transition between two topological phases [14,15]. For the latter, the usual definitions of topological invariants become ill-defined. A general recipe for obtaining well-defined invariants for critical systems was first presented in [15], by removing an infinitesimal region around each of the gapless points.

For the winding number, this implies that instead of (4), we use the regularized version

$$\nu_\epsilon = \frac{1}{2\pi} \int_{()} dk \partial_k \arg[h_x(k) - ih_y(k)], \quad (6)$$

where $()$ denotes that we removed a region $[k_c - \epsilon, k_c + \epsilon]$ from the integration around each gapless point k_c . In the limit $\epsilon \rightarrow 0$, ν_ϵ becomes half-integer quantized and is given generically by the mean of the winding numbers on either side of the critical point (for details see Ref. [15]). In particular, at the critical point between gapped phases with winding numbers 0 and 1, respectively, the winding number $\nu_\epsilon \rightarrow \frac{1}{2}$ for $\epsilon \rightarrow 0$.

There is an alternative formulation of the winding number for gapped systems by interpreting f ($=f_1 = f_2^*$) in Eq. (1) as a complex function $f(z = e^{ik})$ and relating the winding number to the difference in numbers of zeros and poles within the unit circle, using Cauchy's argument principle [5,14,37,38],

$$\nu = \frac{1}{2\pi i} \oint dz \frac{f'(z)}{f(z)} = Z - P, \quad (7)$$

where Z and P denote the numbers of zeros and poles, respectively, within the unit circle. This identity is not valid for gapless systems because there is a zero in the contour. One alternative for gapless systems is to again exclude an infinitesimal region around each point z ,

$$\nu_\epsilon = \frac{1}{2\pi i} \oint_{()} dz \frac{f'(z)}{f(z)}. \quad (8)$$

Each zero of order n on the unit circle contributes $n/2$ to the winding number, in agreement with the discussion in the previous above. One could, however, have chosen to define the invariant differently, namely, as $\tilde{\nu} = Z - P$, where Z and P are the zeros and poles strictly within the unit circle, respectively. This instead gives an integer (not half-integer) quantized invariant, which in addition is related to the number of topologically protected edge modes [14,17].

One disadvantage of Verresen's approach in Ref. [15] is that one needs to compute different invariants, depending on whether the system is gapless or gapped; the invariant for gapped systems is ill-defined for gapless ones. A different way of regularizing the winding number for gapless systems was discussed in Ref. [18], namely, by considering the system at finite temperatures. Computing the $T \rightarrow 0$ limit in a gapped system yields (4), while doing the same for a critical system yields the $\epsilon \rightarrow 0$ limit of Eq. (6), as the Boltzmann weights

suppress the contribution in the vicinity of gapless points. It thus has the advantage that gapped and gapless systems can be treated on the same footing. The generalization to non-Hermitian systems detailed in Secs. III and IV can, in some sense, be regarded as yet another regularization of the winding number that treats gapped and gapless systems on the same footing.

Note that the winding number $\lim_{\epsilon \rightarrow 0} \nu_\epsilon$ does not uniquely characterize the critical system, nor is it connected to the number of topologically protected edge modes. Two different critical points, e.g., the phase transitions $\nu = 0 \rightarrow 3$ and $\nu = 1 \rightarrow 2$, have the same value $\nu = \frac{3}{2}$ of the winding number. The first critical point has no protected topological edge modes, while the latter has one. In general, the number of topological edge modes is given by [14]

$$N_{\text{top}} = \begin{cases} \tilde{\nu} & \text{if } \tilde{\nu} > 0 \\ |\tilde{\nu} + N| & \text{if } \tilde{\nu} < -N \\ 0 & \text{otherwise,} \end{cases} \quad (9)$$

where $\tilde{\nu} = Z - P = \nu - N/2$, Z and P are the number of zeros and poles strictly within the unit circle, respectively, and N is the number of zeros (times their multiplicity) on the unit circle. A complete characterization of the critical system thus requires two numbers, e.g., $\tilde{\nu}$ and N . This is very similar to the non-Hermitian point-gap phases discussed below.

B. Non-Hermitian systems with sublattice symmetry

In this paper we focus on systems in symmetry class AI, with a sublattice symmetry S that commutes with time reversal.¹ Such systems are specified by two winding numbers. A commonly used characterization uses winding numbers ν and ν' , where ν is given by Eq. (5) and ν' denotes the winding of the complex energy bands around the origin [5,10] (sometimes referred to as energy vorticity):

$$\nu' = \frac{1}{2\pi} \oint dk \partial_k \arg[\sqrt{h_x(k)^2 + h_y(k)^2}]. \quad (10)$$

An alternative formulation was presented in Refs. [5,19]. Since $f_1 \neq f_2^*$ (1) in non-Hermitian systems, we can define two independent winding numbers by

$$\begin{aligned} \nu_1 &= \frac{1}{2\pi i} \int dk \partial_k \ln[f_1(k)], \\ \nu_2 &= -\frac{1}{2\pi i} \int dk \partial_k \ln[f_2(k)], \end{aligned} \quad (11)$$

which fulfill

$$\begin{aligned} \nu &= \frac{1}{2}(\nu_1 + \nu_2), \\ \nu' &= \frac{1}{2}(\nu_1 - \nu_2). \end{aligned} \quad (12)$$

Note that the minus sign in the second of Eqs. (11) ensures that $\nu_1 = \nu_2$ in the Hermitian limit.² An appealing feature of

¹In the notation of Table VII in Ref. [6] we consider systems in AI with S_+ .

²We should note that our conventions differ from those of [19]. Using a tilde to indicate the conventions of the latter, we use $\nu = -\tilde{\nu}$, $\nu' = \tilde{\nu}'$, $\nu_1 = -\tilde{\nu}_2$, and $\nu_2 = -\tilde{\nu}_1$.

the winding numbers $\nu_{1/2}$ is that they are directly related to the presence of topologically protected boundary modes present at the right/left edge of a semi-infinite open system [19]. We will later see that $\nu_{1/2}$ also have a natural interpretation in the connected Hermitian critical system: They can often be identified with the winding numbers of the neighboring gapped phases, which will be discussed in Sec. IV.

C. Entanglement occupancy spectrum

The entanglement spectrum was originally proposed for strongly interacting fractional quantum Hall liquids [39] as a useful tool to obtain information about the topology of the state. It is obtained by first partitioning the system into two parts A and B (usually in real space) and tracing out the degrees of freedom in B to obtain the reduced density matrix $\rho_A = \text{Tr}_B(|\psi\rangle\langle\psi|)$, where $|\psi\rangle$ denotes the ground state of the system. We can now define an entanglement Hamiltonian H_A by

$$\rho_A = e^{-H_A}, \quad (13)$$

whose spectrum is called an entanglement spectrum and contains valuable information about the topological properties of the system.

The entanglement spectrum is also of interest in noninteracting systems, as it is directly connected to the topological edge modes in gapped topological insulators [26]. Peschel showed that for noninteracting systems one does not need to compute the full many-body entanglement spectrum (a difficult task even for noninteracting systems) [24]. Instead, one can obtain the same information from the spectrum of the reduced correlation matrix

$$C_{j,j',\alpha,\beta}^A = \langle \text{gs} | c_{j,\alpha}^\dagger c_{j',\beta} | \text{gs} \rangle, \quad (14)$$

where α and β denote internal degrees of freedom and j and j' denote sites in region A . In the following, we will call the spectrum of C^A the EOS. Topological states correspond to $\xi = \frac{1}{2}$ modes of the EOS, since these give rise to degeneracies in the many-body entanglement spectrum. The number of $\xi = \frac{1}{2}$ modes is identical to the number of topologically protected edge modes (see Ref. [26]).

The correlation matrix spectrum for non-Hermitian systems was first studied in Ref. [31]. Since left and right eigenstates are not equivalent anymore, there are in principle three distinct versions of Eq. (14), using either the left-left, right-right, or left-right ground states. As argued in [31], the left-right choice is usually the one that behaves best and which we use throughout the paper. Numerical simulations suggest that the topological features of the EOS for line gap phases are similar to those of Hermitian gapped phases. In particular, one finds a one-to-one correspondence between the topological zero-energy states in the open system and the $\xi = \frac{1}{2}$ modes in the EOS. For a sublattice symmetric model with winding number ν there will be 2ν topological zero-energy modes, ν on each edge, and the same number of $\frac{1}{2}$ modes in the EOS.

Focusing on two-band models with sublattice symmetry as in (1), an intuitive way of arguing for this is the following: The correlation matrix in momentum space can be written as

$$C(k) = \frac{1}{2}[\mathbf{1} + Q(k)], \quad (15)$$

where $Q(k)$ is given by

$$Q(k) = \begin{pmatrix} 0 & -\sqrt{f_1(k)/f_2(k)} \\ -\sqrt{f_2(k)/f_1(k)} & 0 \end{pmatrix}, \quad (16)$$

using the explicit form of the left and right eigenvectors in (2) and (3). We can choose the branch cuts of the square root in such a way that $Q(k)$ is continuous and differentiable. In addition, it is 2π periodic in k . Thus, we can interpret Q as a Hamiltonian with sublattice symmetry and compute the winding number relevant for line-gapped systems,

$$\begin{aligned} \nu &= \frac{1}{2\pi i} \int_0^{2\pi} dk \partial_k \ln \sqrt{f_1(k)/f_2(k)} \\ &= \frac{1}{2} \frac{1}{2\pi i} \int_0^{2\pi} dk \partial_k [\ln f_1(k) - \ln f_2(k)] \\ &= \frac{1}{2} (\nu_1 + \nu_2). \end{aligned} \quad (17)$$

Since the system is line gapped, $\nu_1 = \nu_2 = \nu$ and $Q(k)$ has the same winding number as the original Hamiltonian. Computing C^A amounts to computing the real-space Fourier transform of Q in region A . The latter harbors 2ν topological zero modes, resulting in $2\nu, \frac{1}{2}$ modes in the EOS using Eq. (15).

The situation for Hermitian critical and non-Hermitian point-gap phases is more complicated. An imminent problem is that it is not clear which ground state to use in (14). Numerical simulations show that for point-gapped systems, the EOS seems to harbor $\min(N_L, N_R), \frac{1}{2}$ modes, where N_L and N_R are the topological zero modes of a semi-infinite system [40]. In addition, these topological features were seen to be insensitive to the particular choice of ground state, while nontopological modes may be affected. In our numerical simulations, the same seems to hold for critical systems, where now $N_L = N_R$ are the number of topologically protected edge modes on the left/right edge in the open boundary system. We will comment more on this in Sec. V, where we will also prove the equivalence of the EOS between Hermitian critical and non-Hermitian point-gapped phases for simple yet nontrivial cases.

III. GENERALIZING EIGENENERGIES

As we mention in the Introduction, the aim of this paper is to show the connection in the topological features of critical Hermitian models and point-gapped non-Hermitian ones. In order to do that we first start with Hermitian models at a critical point and deform them to become non-Hermitian, showing that the topological features remain unchanged by this deformation. We consider two distinct ways of deforming the Hermitian critical system. The first and simpler approach, discussed in this section, amounts to making eigenenergies complex while keeping the eigenstates unchanged. Since we do not modify the eigenstates, the left and right non-Hermitian eigenstates are still equal to each other and one can use all the usual techniques in Hermitian quantum mechanics. To further simplify the discussion, we only consider critical systems where the gapless points are zeros of order 1. Generalizing to higher orders is straightforward. A less restrictive

generalization, which also modifies the eigenstates, is discussed in Sec. IV.

For a given Hermitian Hamiltonian, written in the eigenbasis

$$H = \sum_{k\mu} \varepsilon_{k\mu} |\psi_{k\mu}\rangle \langle \psi_{k\mu}|, \quad (18)$$

the eigenenergies are modified by adding the perturbation

$$\begin{aligned} H(g) &= \sum_{k\mu} \varepsilon_{k\mu}(g) |\psi_{k\mu}\rangle \langle \psi_{k\mu}| \\ &= \sum_{k\mu} (\varepsilon_{k\mu} + ig \partial_k \varepsilon_{k\mu}) |\psi_{k\mu}\rangle \langle \psi_{k\mu}|, \end{aligned} \quad (19)$$

where $\varepsilon_{k\mu}$ are the energies of the Hermitian system, μ is the band index, and $\partial_k \varepsilon_{k,\mu}$ is by assumption nonzero. By construction, the eigenstates remain intact. As will be shown below, this generalization results in a point-gapped Hamiltonian. However, we first want to illustrate this generalization by the simplest possible example, assuming eigenenergies $\varepsilon_{k,\mu} = \pm \sin(k/2)$ with a single gapless point at $k = 0$. In order to construct the resulting complex band structure, it is easier to regard the model as an effective one-band model in an extended Brillouin zone $k \in [-2\pi, 2\pi)$. The resulting complex energies are

$$\tilde{\varepsilon}_k(g) = \sin(k/2) + i \frac{g}{2} \cos(k/2), \quad (20)$$

which is nothing but the parametric equation of an ellipse in the complex plane. The system has therefore a point-gap around zero. More generally, zeros of the Hermitian model correspond to crossings of the imaginary axis (with a finite imaginary part), while maxima and minima correspond to crossings of the real axis.

In terms of the Hamiltonian (1), the generalization in (19) can be written as

$$H(k, g) = \varepsilon(k, g) \hat{h}(k) \cdot \sigma = [\varepsilon(k) + ig \partial_k \varepsilon(k)] \hat{h}(k) \cdot \sigma, \quad (21)$$

with both $\varepsilon(k)$ and $\hat{h}(k)$ continuous and differentiable. This can always be done for finite-range hopping Hamiltonians. Even though $\hat{h}(k)$ is not uniquely defined at a gapless point k_c , there is a consistent limit

$$\lim_{\delta \rightarrow 0} \hat{h}(k_c + \delta) = \lim_{\delta \rightarrow 0} \hat{h}(k_c - \delta) \quad (22)$$

as long as $\varepsilon(k)$ changes sign at k_c (for a single zero). For explicit examples on how to choose $\varepsilon(k)$ and $\hat{h}(k)$, we refer the reader to Appendix A.

We now proceed to compute the winding number ν for the original, critical Hamiltonian $H(k, 0)$, using the conventions of (21). A short calculation shows that ν only depends on \hat{h} , but not on ε ,

$$\begin{aligned} \nu_\varepsilon &= \frac{1}{2\pi} \int_0^{2\pi} dk \frac{[\partial_k h_x(k)] h_y(k) - h_x(k) \partial_k h_y(k)}{h_x(k)^2 + h_y(k)^2} \\ &= \frac{1}{2\pi} \int_0^{2\pi} dk \frac{\varepsilon(k)^2 (\hat{h}'_x \hat{h}_y - \hat{h}_x \hat{h}'_y)}{\varepsilon(k)^2} \\ &\rightarrow \frac{1}{2\pi} \int dk (\hat{h}'_x \hat{h}_y - \hat{h}_x \hat{h}'_y) \quad \text{for } \varepsilon \rightarrow 0, \end{aligned} \quad (23)$$

where we abbreviated $\partial_k \hat{h}_\alpha = \hat{h}'_\alpha$. The last equality is valid as long as the integrand is regular, i.e., neither \hat{h} or \hat{h}' has singularities at the gapless points of the critical system. This is trivially satisfied for the finite-range hopping models usually considered. The resulting winding number is half-integer quantized (see [15]). Repeating the same computation for the non-Hermitian Hamiltonian, we find that the winding number

$$\begin{aligned} \nu(g) &= \frac{1}{2\pi} \int dk \frac{[\partial_k h_x(k, g)] h_y(k, g) - h_x(k, g) \partial_k h_y(k, g)}{h_x(k, g)^2 + h_y(k, g)^2} \\ &= \frac{1}{2\pi} \int dk \frac{\epsilon(k, g)^2 (\hat{h}'_x \hat{h}_y - \hat{h}_x \hat{h}'_y)}{\epsilon(k, g)^2} \\ &= \frac{1}{2\pi} \int dk (\hat{h}'_x \hat{h}_y - \hat{h}_x \hat{h}'_y) \end{aligned} \quad (24)$$

is again independent of ϵ (and thus g) and equal to the last line of (23). This shows that the generalization of the critical system to the non-Hermitian one does not alter the winding number ν .

We can now continue taking a look at the second non-Hermitian winding number

$$\nu' = \frac{1}{2\pi} \oint_0^{2\pi} dk \partial_k \text{Im} \log \det[h(k, g)], \quad (25)$$

which is equivalent to the phase winding of one of the energy bands. In order to use the form of Eq. (21), it is advantageous to compute $2\nu'$ by extending the integration from 0 to 4π , thus allowing us to consider $\epsilon(k, g)$ as one of the energy bands. In order to compute the winding, we now count the crossings at the positive imaginary axis (with an additional sign depending on the orientation). We will now show that the contribution of all gapless points to the winding number sums up, with only an overall sign depending on the sign of g . Let us fix the sign of g to be positive and focus on one of the gapless points, denoted by k_c . If $\partial_k \epsilon(k) > 0$, the crossing happens on the positive imaginary part from $\text{Re}[\epsilon(k_c - \delta)] < 0$ to $\text{Re}[\epsilon(k_c + \delta)] > 0$. If instead $\partial_k \epsilon(k) < 0$, the crossing happens on the negative imaginary part from $\text{Re}[\epsilon(k_c - \delta)] > 0$ to $\text{Re}[\epsilon(k_c + \delta)] < 0$, i.e., it has the same orientation as above. Thus, the contributions of all gapless points simply add up with a positive sign. Switching the sign of g , switches the orientation. Thus, the winding number ν' is given by

$$\nu' = \text{sgn}(g)N/2, \quad (26)$$

where N is the total number of zeros, without multiplicity, and the $\frac{1}{2}$ factor is because our previous argument was made for $2\nu'$. Clearly, ν' itself is not well defined in the $g \rightarrow 0$ limit, though its absolute value is and simply counts the number of gapless points.

IV. GENERALIZATION TO COMPLEX MOMENTUM

In the preceding section we have shown a method for obtaining a point-gapped phase from a Hermitian critical system that can be used to relate the topology of both models. However, the generalization considered, modifying only the eigenvalues and not the eigenstates, is overly simplistic and artificial. A more realistic generalization one can make is by performing an analytical continuation of the momenta

in the Bloch Hamiltonian into the complex plane, $H(k) \rightarrow H(k, g) = H(k - ig)$. For a Hermitian model, a general Bloch Hamiltonian with sublattice symmetry can be written as

$$H(k) = \begin{pmatrix} 0 & f \\ f^* & 0 \end{pmatrix}, \quad f = \sum_n t_n e^{ikn}, \quad (27)$$

where t_n are all possible hoppings. The non-Hermitian generalization reads

$$H(k, g) = \begin{pmatrix} 0 & \sum_n t_n e^{gn} e^{ikn} \\ \sum_n t_n^* e^{-gn} e^{-ikn} & 0 \end{pmatrix}. \quad (28)$$

It is equivalent to introducing nonreciprocity in the intercell hopping terms, which is a common way of introducing non-Hermiticity. Adding nonreciprocity generically leads to an unbalanced hopping resulting in the skin effect, where for open boundary conditions electrons accumulate at one of the boundaries. The skin effect is a characteristic property of point-gapped phases, and the expectation is that the perturbation (28) will evolve the critical system into a point-gapped phase. We will see below that this is indeed the case.

Before continuing, let us consider g as a small perturbation

$$\begin{aligned} H(k, g) &= \mathbf{h}(k, g) \cdot \boldsymbol{\sigma} \\ &= h(k, g) \hat{h}(k, g) \cdot \boldsymbol{\sigma} \\ &\approx \{h(k) \hat{h}(k) + g[\partial_g h(k, g)|_{g=0}] \hat{h}(k) \\ &\quad + gh(k) \partial_g \hat{h}(k, g)|_{g=0}\} \cdot \boldsymbol{\sigma}. \end{aligned} \quad (29)$$

Using that $\partial_g \mathbf{h}(k, g) = -i \partial_k \mathbf{h}(k, g)$,

$$\begin{aligned} H(k, g) &\approx [h(k) - ig \partial_k h(k)] \hat{h}(k) \cdot \boldsymbol{\sigma} \\ &\quad - igh(k) \partial_k \hat{h}(k) \cdot \boldsymbol{\sigma}, \end{aligned} \quad (30)$$

we note that the first term is exactly the generalization considered in the preceding section (up to the unimportant sign of g), but we now obtain a second term that also modifies the eigenvectors. Therefore, in the perturbative limit the two generalizations may be similar, though not identical. More specifically, they connect to the same phase as long as the critical system has no zeros with multiplicity $n > 1$.

In contrast to the first generalization to non-Hermitian systems considered in Sec. III, it is now much easier to compute the winding numbers $\nu_{1/2}$ and then use their relation to ν and ν' (12) to connect the result to the critical system. We begin by rewriting the expression for winding number ν_1 in (11) in the complex plane, employing $z = e^{ik}$ as the holomorphic variable

$$\nu_1 = \frac{1}{2\pi i} \oint_{|z|=1} dz \partial_z \ln[f(ze^{-g})] \quad (31)$$

and using $f(z) = \sum_n t_n z^n$, i.e., the appropriate expression for the critical system. We can absorb the scale factor by a change of variables $z' = ze^{-g}$ and obtain

$$\nu_1(g) = \frac{1}{2\pi i} \int_{|z'|=e^{-g}} dz' \partial_{z'} \ln[f(z')], \quad (32)$$

which can now be obtained as $\nu_1 = Z_1 - P_1$, where Z_1 and P_1 are the zeros and poles, respectively, of $f(z)$ inside the circle $|z| = e^{-g}$ (times their multiplicity). Note that, for the

Hamiltonian considered here,

$$f(z) = \sum_{n=-l}^r t_n z^n = \frac{P_{l+r}(z)}{z^l} \quad (33)$$

is a polynomial with $P = l$ poles at zero and $l + r$ zeros. For most of the commonly used model Hamiltonians, $l = 0$ (e.g., the extension of the SSH model used in Appendix A or the Hatano-Nelson model), but this is by no means a prerequisite.

For v_2 we perform exactly the same steps, after substituting $k' = -k$ so that f_2 becomes a holomorphic, not antiholomorphic, function after expressing $z = e^{ik'}$:

$$\begin{aligned} v_2 &= \frac{1}{2\pi i} \int_0^{2\pi} dk' \partial_{k'} \ln f(z e^g) \\ &= \frac{1}{2\pi i} \oint_{|z|=1} dz \partial_z \ln[f(z e^g)]. \end{aligned} \quad (34)$$

We can again absorb the scale factor by a change of variables, but now we set $z' = z e^g$ instead. Consequently, v_2 is given by $v_2 = Z_2 - P_2$, where Z_2 and P_2 are now the zeros and poles, respectively, of $f(z)$ inside the circle $|z| = e^g$.

For infinitesimal $g > 0$, v_1 counts $(Z - P)$ for all zeros and poles that lie strictly within the unit circle $v_1 = \tilde{v}$, while v_2 even counts the zeros that lie on the unit circle. Assuming we do not go through any phase transition when enlarging g , the difference of the two winding numbers is simply the number of zeros of $f(z)$ on the unit circle times their multiplicity,

$$v_1(g) - v_2(g) = N = 2v'. \quad (35)$$

When the underlying critical system has only single zeros, this is consistent with our previous results (26).³ Interestingly, as long as we look at phase transitions where zeros do not move simultaneously into and out of the unit circle, v_1 and v_2 also correspond to the winding numbers of the gapped Hermitian phases surrounding the gapless point. However, this interpretation of v_1 and v_2 depends on our particular generalization from critical to non-Hermitian systems and will not hold in general.

In order to illustrate this, we consider a very small anti-Hermitian perturbation to our Hamiltonian such that

$$\begin{aligned} f_1(k) &= f(k) + \delta, \\ f_2(k) &= f(k) - \delta^*. \end{aligned} \quad (36)$$

Nonzero δ will generically move the complex zeros either into or out of the unit circle. Let us first consider v_1 and observe that since $f(z)$ has a zero on the unit circle, we can write $f_1(z)$ as

$$f_1(z) = A(z)(z - z_0) + \delta, \quad (37)$$

where z_0 denotes the position of the gapless point. Given that δ is small, we can approximate $A(z)$ by a constant in the

³In the case in which the critical system has zeros with higher multiplicity, the two generalizations to non-Hermitian systems are *not* equivalent, as (26) only depends on the number of zeros, but not their multiplicity. This is a direct consequence of the generalization in Sec. III being too simplistic.

environment of z_0 , yielding

$$f_1(z) \approx A(z_0)[z - z_0 + \delta/A(z_0)] \quad (38)$$

for $z \approx z_0$. Similarly, for the other winding number we have

$$f_2(z) \approx A(z_0)[z - z_0 - \delta^*/A(z_0)]. \quad (39)$$

From these expressions we can now deduce how the zeros move. In the case where δ is real, the zero of one of the functions moves inside the unit circle while the other one moves out, depending on the sign of $\delta/A(z_0)$. This results in v_1 and v_2 being the winding numbers of the gapped neighboring phases of the gapless point. That is no longer the case for purely imaginary δ , as both zeros move in the same direction.

V. ENTANGLEMENT OCCUPANCY SPECTRUM

In this section we show some rigorous results on the EOS for the non-Hermitian generalizations considered above.

A. EOS for generalizing eigenenergies

In this simple case it is trivial to see that the EOS is independent of g , the non-Hermitian parameter. This is because the EOS only depends on the occupied eigenstates, which are not modified by this particular generalization. If we choose to occupy the same eigenstates, independently of g , then the Hermitian and non-Hermitian models will share the same EOS. Furthermore, since the real part of the energies is also independent of g , the common choice of occupying the states with $\text{Re}(\varepsilon_{k\mu}) < 0$ will lead to the same EOS.

When extending the critical model to non-Hermitian phases, we note that \tilde{v} in Eq. (9) becomes identical to v_1 (v_2) for sufficiently small $g > 0$ ($g < 0$). The second important quantity, the number of gapless points on the unit circle N , is encoded in $|v'| = |v_1 - v_2|/2$. For the non-Hermitian phases that are of current interest, $v_{1/2} \geq 0$, which explains their identification with the number of left/right topological edge states in Ref. [19]. However, this identification will fail if one or both of the winding numbers are negative, and one needs to revert to arguments similar to those used in Ref. [14] to derive the correct number of topological edge modes. In general, extensive numerical simulations suggest that the number of topological 1/2 states in the EOS is equal to $\min(N_L, N_R)$, where $N_{L/R}$ are the number of edge modes in the semi-infinite chain (see Ref. [40]). In the limit of the Hermitian critical system, this reduces to Eq. (9). Note that even though the second non-Hermitian winding number v' does not have a well-defined Hermitian limit, its absolute value $|v'| = N/2$ still carries topological information.

B. EOS for generalizing to complex momenta

Making the momenta complex, $k \rightarrow k - ig$, modifies the eigenenergies in a similar way to our first generalization [see, e.g., (30)], but it will also modify the eigenstates. So it is far from obvious that the EOS will remain qualitatively unchanged by this generalization.

In the following we show how the number of topological eigenvalues in the EOS remains unchanged by the non-Hermiticity. To do so, instead of the correlation matrix C , we

consider the matrix

$$Q = 2C - I \quad (40)$$

[see Eq. (16)]. The spectrum of the subsystem matrix Q^A is equivalent to the EOS, with the virtual topological states having zero eigenvalue.

For critical systems, the ground state is degenerate and Q generally depends on the particular ground state chosen. For systems with only one gapless point at k_c , there is a well-defined procedure to choose the ground state by filling either the + or the - band from (2) for $k \in (k_c, k_c + 2\pi]$.⁴ Using this choice of ground state, the momentum space representation of Q becomes

$$Q(k) = \begin{pmatrix} 0 & -e^{i\phi(k)} \\ -e^{-i\phi(k)} & 0 \end{pmatrix}, \quad (41)$$

where $e^{i\phi(k)} = \sqrt{f(k)/f^*(k)}$. Note that $\phi(k)$ is *not* necessarily 2π periodic, in contrast to Hermitian gapped or non-Hermitian line-gapped phases. Inspecting the explicit form of the eigenstates (2) reveals that $\phi(k)$ is 2π periodic for gapped systems, as well as critical systems with an even number of zeros (counting their multiplicity), while for an odd number of zeros it is 4π periodic, as $v_+(k + 2\pi) = v_-(k)$. After the non-Hermitian generalization, the Q matrix becomes

$$Q(k, g) = \begin{pmatrix} 0 & -e^{i\phi(k-ig)} \\ -e^{-i\phi(k-ig)} & 0 \end{pmatrix}. \quad (42)$$

We express the subsystem matrix in position space as

$$Q^A(g) = \begin{pmatrix} -0 & q^A(g) \\ \tilde{q}^A(g) & 0 \end{pmatrix}, \quad (43)$$

where

$$q_{xy}^A(g) = \frac{1}{L} \sum_k e^{ik(x-y)} e^{i\phi(k-ig)}, \quad (44)$$

$$\tilde{q}_{xy}^A(g) = \frac{1}{L} \sum_k e^{ik(x-y)} e^{-i\phi(k-ig)}, \quad (45)$$

and $x, y \in [1, L/2]$. We will now show that assuming that for the critical system there exists an (approximate) zero-energy state of $Q^A(g=0)$, localized at one of the edges, there also exists an (approximate) zero-energy state at $Q^A(g \neq 0)$, again localized at the edge.

We start by assuming that the critical system harbors a zero-energy state $|\psi(0)\rangle$ that is localized on the left edge near $x=1$, with only support on the b sublattice. (The discussion of localized states on the other edge, localized on the a sublattice, can be found in Appendix B.) This is the case for the Hamiltonian of critical semi-infinite chains [14,17]. Our numerics suggests that this is also valid for the EOS.

For a finite size the topological states are not exactly at zero, but one can always construct a state with only support on the b sublattice such that

$$|Q^A(0)|\psi(0)\rangle = O(1/L^2). \quad (46)$$

Given a finite g and Eq. (46), we can construct the state $|\psi(g)\rangle$ such that

$$|Q^A(g)|\psi(g)\rangle \leq \text{const} \times |Q^A(0)|\psi(0)\rangle \quad (47)$$

holds. For a general non-Hermitian matrix, the equation above does not guarantee that the matrix has an eigenvalue close to zero in the thermodynamic limit. However, since there is no skin effect in the EOS, it is reasonable to expect that $O(1/L)$ effects also vanish for the non-Hermitian case. This is also confirmed by our numerical simulations.

In order to simplify the notation, we express the state with support only on the b sublattice as

$$|\psi(g)\rangle = \begin{pmatrix} 0 \\ |u(g)\rangle \end{pmatrix} \quad (48)$$

and the eigenvalue equation reduces to

$$q^A(g)|u(g)\rangle \approx 0. \quad (49)$$

1. Case I: Gapped systems

Before proceeding with critical systems it is worth considering a simpler case first: gapped systems, where q^A is 2π periodic. In this case, we can expand the exponential as a Fourier series, given by

$$e^{i\phi(k)} = \sum_{m=-\infty}^{\infty} \gamma_m e^{ikm}. \quad (50)$$

For a gapped system $\phi(k)$ is continuously differentiable and thus the Fourier series converges. However, we need to additionally require that the coefficients γ_m decay exponentially for large m and that $|g|$ is sufficiently small such that even $\gamma_m e^{gm}$ decays exponentially. We confirmed numerically that the coefficients $\gamma_m e^{|g|m}$ decay exponentially for the short-range hopping model considered here, (A1).

Plugging this expression into Eq. (44), assuming $g > 0$, and evaluating the sum, we find that

$$q_{xy}^A(g) = \gamma_{y-x} e^{g(-x+y)}. \quad (51)$$

Inserting this expression in the eigenvalue equation, we obtain

$$\langle x|Q^A(g)|\psi(g)\rangle = - \sum_{y \in A} \gamma_{y-x} e^{-g(x-y)} u_y(g). \quad (52)$$

We now use the (unnormalized) ansatz $|\psi(g)\rangle = e^{-gx} |\psi(0)\rangle$, where $|\psi(0)\rangle$ is the approximate zero eigenstate of $Q^A(0)$,

$$\begin{aligned} \langle x|Q^A(g)|\psi(g)\rangle &= -e^{-gx} \sum_{y \in A} \gamma_{y-x} u_y(0) \\ &= e^{-gx} \langle x|Q^A(0)|\psi(0)\rangle. \end{aligned} \quad (53)$$

Since e^{-gx} is bounded from above for $x \in [1, L/2]$, we find that

$$\langle x|Q^A(g)|\psi(g)\rangle \leq \text{const} \times \langle x|Q^A(0)|\psi(0)\rangle \quad (54)$$

and thus Eq. (47) is satisfied and the ansatz is an approximate zero eigenstate of $Q^A(g)$ in the line-gapped phase. The exponential factor in the ansatz may seem problematic for $g < 0$, even though our numerics shows that it is not, at least for the simple model Hamiltonian considered here. The proper way

⁴This choice ensures that the Resta polarization behaves consistently with the $T \rightarrow 0$ limit of finite-temperature computations [18].

to deal with $g < 0$ is to consider the left eigenstate of $Q^A(g)$ (see, e.g., the discussion for the gapless case below).

2. Case 2: Critical systems with a single zero

We now consider the case where $\phi(k + 2\pi) = \phi(k) + \pi$. In this case the exponential can be decomposed as

$$e^{i\phi(k)} = e^{ik/2} \sum_{m=-\infty}^{\infty} \gamma_m e^{ikm}. \quad (55)$$

For a system with only a single zero, we can again choose the branch cuts such that $\phi(k)$ is continuously differentiable in the interval $(k_c, k_c + 2\pi]$, where k_c denotes the gapless point. This ensures that the Fourier series converges. However, as in the discussion above, we need to require that the coefficients γ_m decay exponentially for large $|m|$, which is the case for the critical lines in the model system used in Appendix A 1. The non-Hermitian generalization can then be written as

$$e^{i\phi(k-ig)} = e^{i(k-ig)/2} \sum_{m=-\infty}^{\infty} \gamma_m e^{i(k-ig)m}, \quad (56)$$

and we require $|g|$ to be sufficiently small such that $\gamma_m e^{gm}$ still decays exponentially for large $|m|$. This allows us to truncate the sum at large $|m|$, up to errors that are exponentially small in $|m|$.

We look again at the matrix $q^A(g)$, with elements

$$\begin{aligned} q_{xy}^A(g) &= \frac{1}{L} \sum_k e^{ik(x-y)} e^{i\phi(k-ig)} \\ &= e^{g/2} \sum_{m=-\infty}^{\infty} e^{gm} \gamma_m \left(\frac{1}{L} \sum_k e^{ik(m+x-y+1/2)} \right). \end{aligned} \quad (57)$$

We can identify the expression in large parentheses as a matrix with dimensions $L \times L/2$,

$$M_{m,y} = \frac{1}{L} \sum_k e^{ik(m-y+1/2)}, \quad (58)$$

where $y \in [1, L/2]$, whereas m is defined modulo L . The matrix M is well defined and invertible (see Appendix C. Now q^A can be written as

$$\begin{aligned} q_{xy}^A(g) &= e^{g/2} \sum_{m=-\infty}^{\infty} e^{gm} \gamma_m M_{m+x,y} \\ &= e^{g/2} \sum_{m=-\infty}^{\infty} e^{g(m-x)} \gamma_{m-x} M_{m,y} \\ &= e^{g/2} \sum_{m=1}^L \sum_{j=-\infty}^{\infty} e^{g(m-x+jL)} \gamma_{m-x+jL} M_{m,y}, \end{aligned} \quad (59)$$

where in the last step we use that $M_{m+L,y} = M_{m,y}$.

We now assume $g > 0$ and consider the (unnormalized) ansatz

$$u_y(g) = \sum_{s=1}^L \sum_{y'=1}^{L/2} M_{y,s}^{-1} e^{-gs} M_{s,y'} u_{y'}(0), \quad (60)$$

where again $|\psi(g)\rangle = [0, |u(0)\rangle]^T$ is the approximate zero-energy eigenstate of $Q^A(0)$. The state $|u(g)\rangle$ is also localized

to the edge $x = 1$ and exists on the same sublattice as $|u(0)\rangle$. Acting with $Q^A(g)$ on this state $|\psi(g)\rangle$ gives

$$\begin{aligned} -\langle x | Q^A | \psi(g) \rangle &= \sum_{y=1}^{L/2} q_{x,y}^A(g) u_y(g) \\ &= e^{g/2} \sum_{y=1}^{L/2} \sum_{m=-\infty}^{\infty} e^{g(m-x)} \gamma_{m-x} M_{m,y} u_y(g) \\ &= e^{g/2-gx} \sum_{m,s=1}^L \sum_{j=-\infty}^{\infty} e^{g(m+jL)} \gamma_{m-x+jL} \\ &\quad \times \underbrace{\sum_{y=1}^{L/2} M_{m,y} (M^{-1})_{y,s}}_{\delta_{m,s}} e^{-gs} [M | u(0)]_s \\ &= e^{g/2-gx} \sum_{m=1}^L \sum_{j=-\infty}^{\infty} e^{gjL} \gamma_{m-x+jL} [M | u(0)]_m \\ &\approx e^{g/2-gx} \underbrace{\sum_{m=1}^L \gamma_{m-x} [M | u(0)]_m}_{= -\langle x | Q^A(0) | \psi(0) \rangle}. \end{aligned} \quad (61)$$

Going to the last line, we use that terms in the j sum different from $j = 0$ are exponentially small in system size. In order to see this explicitly, we can take a closer look at the j sum. The terms for $j = -1, 0, 1$ are

$$e^{g(jL-x)} \gamma_{m-x+jL} = \begin{cases} e^{-g(L+x)} \gamma_{m-x-L}, & j = -1 \\ e^{-gx} \gamma_{m-x}, & j = 0 \\ e^{g(L-x)} \gamma_{m-x+L}, & j = 1. \end{cases} \quad (62)$$

For $j = -1$ we have the largest terms for $m - x - L \approx 0$, but they are still exponentially suppressed compared to $e^{-gx} \gamma_{m-x}$ due to the exponential e^{-gL} . On the other hand, with $j = 1$ the largest terms are obtained for $m = 1$ and x close to $L/2$ (remember that by assumption the γ_m decay faster than e^{gm} grows). The resulting terms, such as $e^{g(L/2)} \gamma_{1+L/2}$, are still suppressed due to the exponential decay on the γ_m coefficients.

In general, for $j > 0$ we have that

$$|e^{gjL-gx} \gamma_{m-x+jL}| < |e^{g(m+jL-x)} \gamma_{m-x+jL}|,$$

where the latter decays exponentially in system size for large j by assumption. For $j < 0$,

$$|e^{gjL-gx} \gamma_{m-x+jL}| < |\gamma_{m-x+jL}|,$$

where the latter also decays with j exponentially by assumption. As $|\psi(0)\rangle$ is a zero-energy eigenstate of $Q^A(0)$ up to finite-size corrections and the prefactor is bounded from above for $g > 0$, it follows that $|\psi(g)\rangle$ is a zero-energy state of $Q^A(g)$ up to finite-size corrections.

The proof above was done assuming that $g > 0$ and the eigenstates are localized on the left edge. In the case where the eigenstate is localized on the left edge but $g < 0$, we can look at the left eigenstate of Q^A instead,

$$Q^A(g)^\dagger |\psi^L(g)\rangle \approx 0. \quad (63)$$

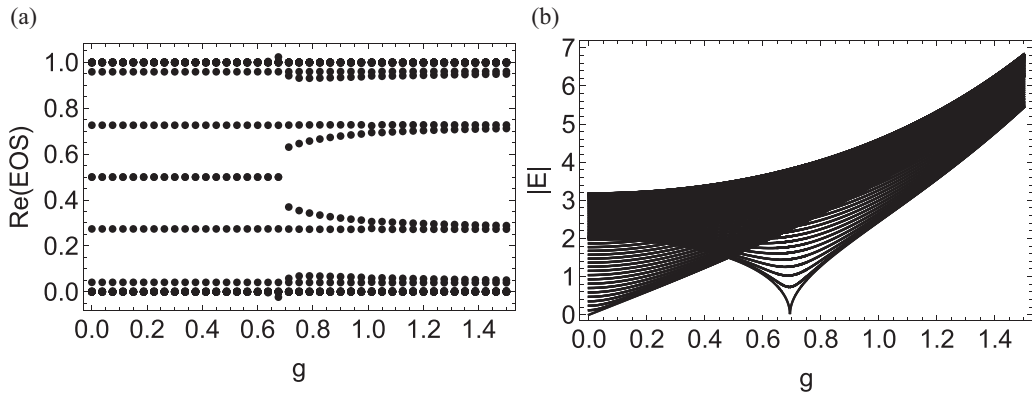


FIG. 1. (a) Real part of the EOS as a function of g , when generalizing the critical Hamiltonian defined by $f(k) = 1 + e^{ik} - 2e^{2ik}$ [see Eq. (1)]. (b) The EOS remains qualitatively unchanged until $g = \ln 2$, where a phase transition to a trivial phase occurs.

As with the right one, the eigenvector is localized on the b sublattice $|\psi^L(g)\rangle = [0, |u^L(g)\rangle]^T$ and the eigenvalue equation reduces to

$$\tilde{q}^A(g)^\dagger |u^L(g)\rangle \approx 0. \quad (64)$$

Comparing $q^A(g)$ and $\tilde{q}^A(g)$ in Eq. (44), we see that

$$\tilde{q}^A(g)^\dagger = q^A(-g). \quad (65)$$

The eigenvalue equation can now be expressed as

$$q^A(-g)^\dagger |u^L(g)\rangle \approx 0, \quad (66)$$

where $-g > 0$. Therefore, the same proof used above for $g > 0$ can be used in this case to show the existence of zero eigenvalues of $Q_A(g)^\dagger$. Since the eigenvalues of $Q_A(g)$ and $Q_A(g)^\dagger$ are related by conjugation, a zero eigenvalue of $Q_A(g)^\dagger$ implies that $Q_A(g)$ also has a zero eigenvalue. The proof for eigenstates localized at the right edge ($x = L/2$) can be found in Appendix B. Apart from the topological modes in the EOS, we generically observe that the rest of the entanglement occupancy spectrum remains qualitatively invariant to the non-Hermitian term, as it can be seen in Fig. 1 for a Hermitian Hamiltonian defined by $f(k) = 1 + e^{ik} - 2e^{2ik}$. This is correct up to the point where non-Hermiticity drives the system to a phase transition, where the EOS changes drastically from the initial Hermitian case.

VI. CONCLUSION

In this paper we have proven analytically that the topological invariants characterizing Hermitian critical systems are the same as those of two distinct generalizations to non-Hermitian point-gap systems. While one of the generalizations also leaves the EOS (a useful tool for characterizing topology) invariant, the other one in general does not. Despite that, numerical simulations strongly suggest that the topological features remain unchanged. We have proven this explicitly for a simple yet nontrivial model. The close relation between Hermitian critical and non-Hermitian point-gapped phases also lends some physical interpretation to some properties of the latter, in particular explaining the number of topological modes in the EOS.

The two non-Hermitian perturbations we considered here are not the only types of perturbation that lead to the same

result. In Appendix D we analyze which types of perturbations drive the system into a gapless phase and which to one of the neighboring gapped phases. In particular, we show that any perturbation that mixes the left- and right-moving states directly at the band crossing results in a line-gapped phase. Perturbations that shift the momenta by an imaginary value $k + ig$ result in a point-gapped phase. Note, however, that this restriction only applies directly at the critical point. Away from the critical point, we can allow mixing of the right and left movers and still obtain a point-gapped phase. The second generalization considered in this paper is a special case of the latter, because it does not mix left and right movers at any momentum.

Our results might be utilized in at least two different ways. We can regard the non-Hermitian generalizations discussed in Secs. III and IV as a regularization of the critical phase, which might prove useful in studying critical systems. It also allows us to compute quantities for non-Hermitian models using Hermitian physics and to address questions regarding critical Hermitian systems using the well-studied topological classification for non-Hermitian systems. The latter has proven useful in finding a physical explanation for the number of virtual edge modes in the EOS of non-Hermitian systems, which in fact is determined by the corresponding Hermitian critical system.

In this paper we focused on one-dimensional systems chiral symmetry, which are characterized by winding numbers. We expect our results to generalize to other topological classes, although a thorough analysis of this is beyond the scope of this paper. In one dimension, the nontrivial critical systems are those with a \mathbb{Z} classification and therefore are covered by the results of this paper. However, more interesting phenomena could appear in higher dimensions. Consider the Chern insulator in topological class A, for example. In the Hermitian case, the critical point is characterized again by a half-integer invariant. As opposed to one dimension, adding a perturbation will generically lead to a gapless phase with exceptional points. We expect that the gapless non-Hermitian phase inherits some of the topological features of the Hermitian critical system.

Note added. Recently, another work was put forward [41] that deals with the relation of non-Hermitian to Hermitian critical systems. However, in [41] the authors relate Hermitian

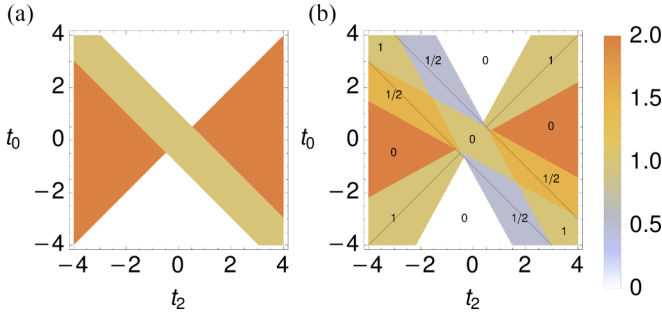


FIG. 2. Phase diagram for the Hamiltonian (A1) with $t_1 = 1$ for (a) $g = 0$ and (b) $g = 0.2$. The color code indicates ν , while the numbers indicate ν' (only nonzero for $g \neq 0$).

critical systems to non-Hermitian critical systems. An important aspect of their construction is that the non-Hermitian energy spectrum is real (and gapless). Thus, their construction is distinct from ours, even though many of the features are similar. In particular, also for point-gap phases, one obtains an entanglement entropy scaling linear in subsystem size, implying critical behavior.

ACKNOWLEDGMENTS

We want to thank Lukas Rødland and Eddy Ardonne for useful discussions. This research was supported by the Swedish Research Council under Grant No. 2017-05162 and the Knut and Alice Wallenberg Foundation under Grant No. 2017.0157.

APPENDIX A: EXPLICIT EXAMPLES

In this Appendix we exemplify some of the statements of the main text. Throughout, we use a simple model Hamiltonian given by

$$H = \mathbf{h}(k) \cdot \boldsymbol{\sigma}, \quad (\text{A1})$$

with

$$h_x(k) = t_0 + t_1 \cos(k) + t_2 \cos(2k)$$

$$h_y(k) = t_1 \sin(k) + t_2 \sin(2k),$$

which implies that

$$f(k) = t_0 + t_1 e^{ik} + t_2 e^{2ik}. \quad (\text{A2})$$

The phase diagram of the Hermitian system is shown in Fig. 2(a). We focus our analysis on four critical points given by

- (i) $\{t_0, t_1, t_2\} = \{0, 1, -1\}$ ($\nu : 1 \rightarrow 2$),
- (ii) $\{t_0, t_1, t_2\} = \{-1, 1, 0\}$ ($\nu : 0 \rightarrow 1$),
- (iii) $\{t_0, t_1, t_2\} = \{-1, 1, -1\}$ ($\nu : 0 \rightarrow 2$),
- (iv) $\{t_0, t_1, t_2\} = \{-\frac{1}{2}, 1, -\frac{1}{2}\}$ (tricritical). (A3)

Without loss of generality, we assume $g > 0$ in the following.

1. Generalizing eigenenergies

Let us first consider the first method, described in Sec. III, on how to connect these critical points to non-Hermitian

point-gap phases. Below we give the analytical expressions for $\epsilon(k, g)$ as well as \hat{h} .

(i) For $\nu : 1 \rightarrow 2$,

$$\begin{aligned} \epsilon(k, g) &= 2 \sin(k/2) + ig \cos(k/2), \\ \hat{h}_x(k) &= \sin(3k/2), \\ \hat{h}_y(k) &= \cos(3k/2). \end{aligned} \quad (\text{A4})$$

(ii) For $\nu : 0 \rightarrow 1$,

$$\begin{aligned} \epsilon(k, g) &= 2 \sin(k/2) + ig \cos(k/2), \\ \hat{h}_x(k) &= -\sin(k/2), \\ \hat{h}_y(k) &= -\cos(k/2). \end{aligned} \quad (\text{A5})$$

(iii) For $\nu : 0 \rightarrow 2$,

$$\begin{aligned} \epsilon(k, g) &= 1 - 2 \cos(k) + 2ig \sin(k), \\ \hat{h}_x(k) &= \cos(k), \\ \hat{h}_y(k) &= -\sin(k). \end{aligned} \quad (\text{A6})$$

(iv) For the tricritical point,

$$\begin{aligned} \epsilon(k, g) &= 1 - \cos(k) + ig \sin(k), \\ \hat{h}_x(k) &= \cos(k), \\ \hat{h}_y(k) &= -\sin(k). \end{aligned} \quad (\text{A7})$$

Note first that whenever there is an odd number of gapless points, $\epsilon(k)$ cannot be chosen as 2π periodic, but must be 4π periodic. This is intimately related to $\hat{h}(k + 2\pi) = -\hat{h}(k)$ and thus a half-integer quantized winding number. The winding numbers of (i) and (ii) are $\frac{3}{2}$ and $\frac{1}{2}$, respectively. For cases (iii) and (iv), we note that both ϵ and \hat{h} are 2π periodic. The corresponding winding number is 1. At first glance, it may be surprising that the winding number of the tricritical point is at all well defined. It is however a fact that appears again in our second non-Hermitian generalization. In the latter, the tricritical point connects to the same point-gapped phase as (iii).

2. Generalizing to complex momenta

We now consider the non-Hermitian generalization of critical systems, obtained by letting the momenta become complex as $e^{ik} \rightarrow e^{ik-g}$. The resulting phase diagram is shown in Fig. 2, with the color code indicating ν and the numbers indicating ν' . Note that increasing g turns the critical line into point-gap phases, while gapped phases smoothly evolve to line-gapped phases (with $\nu' = 0$) as expected [6].

For (i) $\nu : 1 \rightarrow 2$ and using $z = e^{ik}$, f_1 is given by

$$f_1(z) = e^{-g}z - e^{-2g}z^2 = e^{-g}z(1 - e^{-g}z), \quad (\text{A8})$$

which has single zeros at $z = 0$ and $z = e^{ig}$. Thus, the second zero has moved outside the unit circle and the resulting winding number in Eq. (31) evaluates to 1. For f_2 we instead find

$$f_2(z) = e^g z - e^{2g} z^2 = e^g z(1 - e^g z), \quad (\text{A9})$$

with $z = e^{ik'} = e^{-ik}$, which has single zeros at $z = 0$ and $z = e^{-ig}$. Thus the zero has moved inside the unit circle and the resulting winding number [see Eq. (34)] is 2.

For case (ii), f_1/f_2 instead become

$$f_{1/2} = -1 + ze^{\mp g}, \quad (\text{A10})$$

which when compared to (i) above lacks the single zero at $z = 0$, thus yielding $\nu_1 = 0$ and $\nu_2 = 1$ when evaluating the winding number integrals.

For case (iii),

$$\begin{aligned} f_{1/2} &= -1 + ze^{\mp g} - z^2 e^{\mp 2g} \\ &= (z - e^{-\pi i/3} e^{\mp g})(z - e^{i\pi/3} e^{\mp g}); \end{aligned} \quad (\text{A11})$$

thus both zeros move simultaneously either inside or outside the unit circle yielding $\nu_1 = 0$ and $\nu_2 = 2$.

Finally, for case (iv) one finds

$$f_{1/2} = -\frac{1}{2} + ze^{\mp g} - \frac{1}{2}z^2 e^{\mp 2g} = (z - e^{\mp g})^2, \quad (\text{A12})$$

which is completely equivalent to case (iii), except that both zeros now sit at the same point. Again, the winding numbers are given by $\nu_1 = 0$ and $\nu_2 = 2$. In all these cases, the gapless point(s) for each winding number move either all inside or all outside, thus allowing us to identify ν_1 and ν_2 with the gapped phases on each side of the critical point.

APPENDIX B: EOS MIDGAP STATES FOR LOCALIZATION AT $L/2$

Here we discuss the case where the approximate eigenstate exists on the a sublattice and is localized on the edge at $x = L/2$. In this case, we need to ensure that the ansatz for $g \neq 0$ is localized at $L/2$, which is achieved by using

$$\psi_y(g) = \sum_{s=-L/2+1}^{L/2} \sum_{y'=1}^{L/2} M_{y,s}^{-1} e^{g(L/2-s)} M_{s,y'} \psi_{y'}(0), \quad (\text{B1})$$

where we assume that $g < 0$. Note that it is important to change the range of the internal index of M to $[-L/2 + 1, L/2]$. Strictly speaking, this is now a different matrix than in the main text, but we will still call it M . Now we need to Fourier transform $\tilde{q}^A(g)$, which has in fact the same form as q^A just that we replace γ by $\tilde{\gamma}$. If $|\gamma_m|$ is maximal for small positive m , $\tilde{\gamma}$ will be so for small negative m . Otherwise, they share the same features. In particular, we also require the exponential decay for large $|m|$.

Let us now act with Q^A on our ansatz

$$\begin{aligned} -\langle x | Q^A(g) | \psi(g) \rangle &= e^{g/2} \sum_{y=1}^{L/2} \sum_{m=-\infty}^{\infty} e^{g(m-x)} \tilde{\gamma}_{m-x} M_{m,y} \psi_y(g) \\ &= e^{g/2-gx} \sum_{s,m=-L/2+1}^{L/2} \sum_{j=-\infty}^{\infty} e^{g(m+jL)} \gamma_{m-x+jL} \\ &\quad \times \underbrace{\sum_{y,y'=1}^{L/2} M_{m,y} (M^{-1})_{y,s} e^{g(L/2-s)} M_{s,y'}}_{\delta_{m,s}} \psi_y(0) \\ &= e^{g/2+g(L/2-x)} \sum_{m=-L/2+1}^{L/2} \sum_{j=-\infty}^{\infty} e^{gjL} \gamma_{m-x+jL} \\ &\quad \times \sum_y M_{my} \psi_y(0). \end{aligned} \quad (\text{B2})$$

We will now argue that we can restrict the sum to the terms with $j = 0$, making an exponentially small error. First of all, we notice that $e^{gjL} \gamma_{m-x+jL}$ decays exponentially in system size with large $|j|$, independently of m and x . Note that $m - x \in [-L + 1, L/2 - 1]$. We now compare coefficients for different values of $j = -1, 0, 1$,

$$e^{g(jL+L/2-x)} \gamma_{m-x+jL} = \begin{cases} e^{-g(L/2+x)} \gamma_{m-(L+x)}, & j = -1 \\ e^{g(L/2-x)} \gamma_{m-x}, & j = 0 \\ e^{g(3L/2-x)} \gamma_{m+L-x}, & j = 1, \end{cases} \quad (\text{B3})$$

and show that all but the $j = 0$ term can be neglected. Considering $j = -1$, the largest coefficient is generically obtained by choosing $m = L/2$: $e^{-g(L/2+x)} \gamma_{-(L/2+x)}$. Since $x > 0$, and $e^{-gm} \gamma_m$ is assumed to decay exponentially for large $|m|$, this coefficient is exponentially small in system size. For $j = 1$, the largest term is generically obtained for $m = -L/2$: $e^{g(3L/2-x)} \gamma_{L/2-x}$. For the latter, γ can be of order unity for $x \approx L/2$, but the full term is again exponentially suppressed by the extra e^{gL} . As a result, we can truncate the sum over j to the $j = 0$ term, which implies that the second part of the expression is again equal to the eigenvalue equation for $g = 0$:

$$\langle x | Q^A(g) | \psi(g) \rangle = e^{g/2+g(L/2-x)} \langle x | Q^A(0) | \psi(0) \rangle. \quad (\text{B4})$$

Given that the x -dependent factors in front lie in the interval $[0, 1]$, we can conclude that $|\psi(g)\rangle$ is again a zero-energy eigenstate up to finite-size corrections.

For $g > 0$, we instead need to consider the left eigenstate of Q^A , using the same steps as explained in the main text for $g > 0$ and localization at $x = 1$. Again, we find that depending on the sign of g , we can find either right or a left eigenstate of $Q^A(g)$, which has eigenvalue 0 [up to $O(1/L)$ errors].

APPENDIX C: BEHAVIOR OF THE ANSATZ STATE

In this Appendix we study the ansatz used in Eq. (60) and show that it is well behaved. One interesting feature of this ansatz is that the transformation matrix is model independent, depending only on the g parameter. Let us focus first on the M matrix, given again by

$$M_{my} = \frac{1}{L} \sum_k e^{ik(m-y+1/2)}. \quad (\text{C1})$$

This matrix is in fact unitary,

$$\begin{aligned} [M^\dagger M]_{xy} &= \sum_s \left(\frac{1}{L} \sum_{k'} e^{ik'(x-s-1/2)} \right) \left(\frac{1}{L} \sum_k e^{ik(s-y+1/2)} \right) \\ &= \frac{1}{L} \sum_{kk'} \delta_{k,k'} e^{ik'(x-1/2)} e^{ik'(-y+1/2)} \\ &= \frac{1}{L} \sum_k e^{ik'(x-y)} \\ &= \delta_{x,y}, \end{aligned} \quad (\text{C2})$$

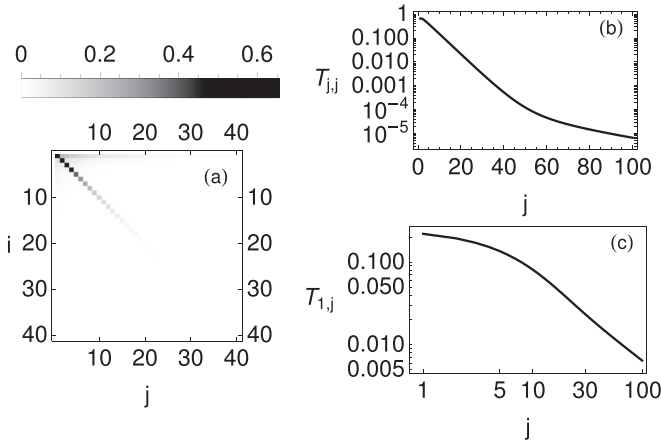


FIG. 3. (a) First 40×40 submatrix of the transformation matrix $T = M^{-1}e^{-gx}M$, computed for $g = 0.2$ and $L = 200$. It has two main features: (b) a diagonal that is exponentially decaying, with the diagonal shown in a log plot, and (c) the first row shown in a log-log plot, pointing to a polynomial decay.

and therefore it is always invertible. The elements of the M matrix can be expressed as

$$\begin{aligned} \frac{1}{L} \sum_k e^{ik(n+1/2)} &= -\frac{1}{L} + \sum_{j=-\infty}^{\infty} \frac{2i}{\pi} \frac{1}{1+2(n+jL)} \\ &= -\frac{1}{L} + \sum_{j=-\Lambda}^{\Lambda} \frac{2i}{\pi} \frac{1}{1+2(n+jL)} \\ &\quad + O\left(\frac{1}{\Lambda L^2}\right), \end{aligned} \quad (\text{C3})$$

where n is an integer and Λ a cutoff. Choosing $\Lambda = 0$ still gives a very good approximation to the correct result in the large-system-size limit, due to the $\frac{1}{L^2}$ dependence of the error.

Despite the simple form of the M matrix, it is not possible to obtain a compact expression for the transformation matrix $T = M^{-1}e^{-gx}M$. We can instead study this transformation matrix numerically, shown in Fig. 3. The transformation matrix has a diagonal that decays exponentially [see Fig. 3(b)]. The rows and columns decay polynomially away from the diagonal [see Fig. 3(c)].

It is now necessary to emphasize certain differences between the topological zero-energy edge modes and the virtual topological modes of the EOS. The former are always exponentially localized at the edge, for both gapped and critical systems. For gapped systems, also the virtual topological modes of the EOS are exponentially localized at the virtual edge. In the critical case, however, we find that they are only polynomially localized, most probably due to the long-range nature of the reduced correlation matrix. Applying the transformation matrix to such a state results in a state that is also polynomially localized, i.e., the transformation does not change the nature of the virtual topological modes. Moreover, in Fig. 4 we plot the norm of the unnormalized ansatz state obtained using the model in Eq. (A1) with $t_0 = t_1$, $t_2 = -2t_1$, and $g = 0.2$, showing that it is well behaved and it converges to a finite number in the thermodynamic limit. Thus, the

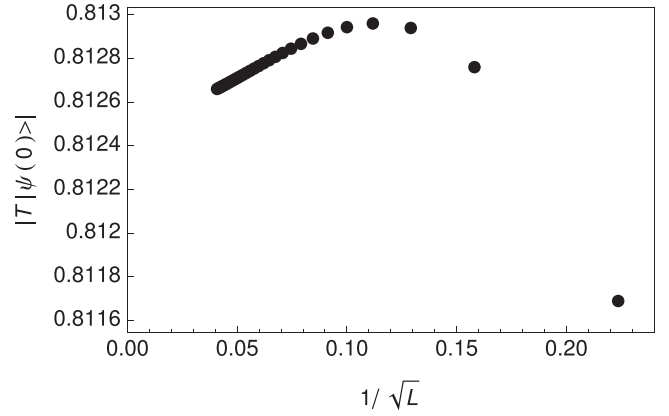


FIG. 4. Norm of the unnormalized ansatz topological state for the model in Eq. (A1) with $t_0 = t_1$ and $t_2 = -2t_1$ for $g = 0.2$ and increasing system size, up to $L = 600$ sites. The ansatz state is well behaved and its norm appears to converge to a finite number in the thermodynamic limit.

ansatz will not cause difficulties in our interpretation of the eigenvalue equation (61).

APPENDIX D: GENERAL NON-HERMITIAN GENERALIZATION

In the main text we described two different generalizations to the non-Hermitian case. These are chosen because they simplify the mathematics and allow us to show analytical results, but the generalizations are not unique. Here we study the requirements for a non-Hermitian term to evolve the critical point into a point-gapped phase by looking at what happens near the band crossing.

Without loss of generality, consider a system with one band crossing at $k = 0$. Near the crossing the Hamiltonian can be expressed in its eigenbasis as

$$H = k\sigma_z, \quad (\text{D1})$$

with left- and right-moving states. Consider first a perturbation of the form

$$H = x\sigma_x + y\sigma_y + k\sigma_z. \quad (\text{D2})$$

Any perturbation like this that mixes left and right movers will result in a line gap opening, even in the non-Hermitian case where x and y are complex. We can see this by calculating the non-Hermitian winding number in Eq. (25),

$$\begin{aligned} \nu' &= \frac{1}{2\pi} \oint_{-\infty}^{\infty} dk \partial_k \text{Im} \log \det[h(k, g)] \\ &= \frac{1}{2\pi} \text{Im} \oint_{-\infty}^{\infty} dk \frac{2k}{k^2 + x^2 + y^2} \\ &= 0, \end{aligned} \quad (\text{D3})$$

where the integration now takes place over the real axis. The winding number vanishes since the integrand is an odd function of k .

This leaves us with only one type of perturbation,

$$H = (k + ig)\sigma_z, \quad (\text{D4})$$

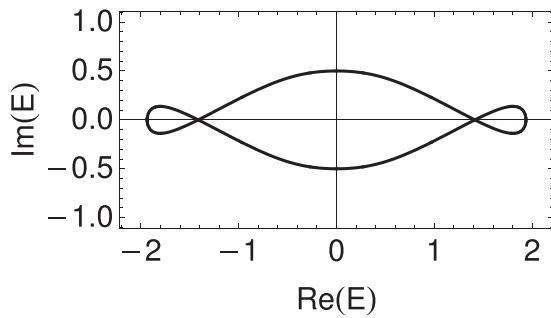


FIG. 5. Energy bands in the complex plane for the Hamiltonian in Eq. (D5) with $g = \frac{1}{2}$ for the perturbation constant, resulting in a point-gapped phase around $E = 0$.

which separates left and right movers in the complex energy plane without mixing them. The corresponding non-Hermitian winding number can be obtained as $\nu' = -\text{sgn}(g)$ [42] and therefore for finite g the system will be in a point-gapped phase. This is expected because the $ig\sigma_z$ term gives different dissipation to left and right movers, which creates

an unbalance in the transport. For open boundary conditions this will lead to a skin effect [43], which is characteristic of point-gapped phases.

In this approximation this is equivalent to the second case considered in the main text, but it only needs to apply exactly at the band crossing. To exemplify this, consider once again the critical point of the SSH chain, with an added perturbation $ig \cos(k)\sigma_y$,

$$H = \begin{pmatrix} 0 & 1 - e^{ik} + g \cos(k) \\ 1 - e^{-ik} - g \cos(k) & 0 \end{pmatrix}. \quad (\text{D5})$$

Near the band crossing at $k = 0$ we have

$$H = \begin{pmatrix} 0 & -i(k + ig) \\ i(k + ig) & 0 \end{pmatrix}, \quad (\text{D6})$$

which is the desired result. Even though the perturbation might mix both bands at other points in k , as long as the perturbation is smaller than the band gap at k , the resulting complex bands should have a point gap. We show that this is the case for the example considered here in Fig. 5.

-
- [1] A. Altland and M. R. Zirnbauer, Nonstandard symmetry classes in mesoscopic normal-superconducting hybrid structures, *Phys. Rev. B* **55**, 1142 (1997).
- [2] A. P. Schnyder, S. Ryu, A. Furusaki, and A. W. W. Ludwig, Classification of topological insulators and superconductors in three spatial dimensions, *Phys. Rev. B* **78**, 195125 (2008).
- [3] A. W. W. Ludwig, Topological phases: Classification of topological insulators and superconductors of non-interacting fermions, and beyond, *Phys. Scr.* **2016**, 014001 (2016).
- [4] D. Bernard and A. LeClair, in *Statistical Field Theories*, edited by A. Cappelli and G. Mussardo, NATO Science Series II: Mathematics, Physics and Chemistry (Springer, Dordrecht, 2002), Vol. 73, pp. 207–214.
- [5] Z. Gong, Y. Ashida, K. Kawabata, K. Takasan, S. Higashikawa, and M. Ueda, Topological Phases of Non-Hermitian Systems, *Phys. Rev. X* **8**, 031079 (2018).
- [6] K. Kawabata, K. Shiozaki, M. Ueda, and M. Sato, Symmetry and Topology in Non-Hermitian Physics, *Phys. Rev. X* **9**, 041015 (2019).
- [7] H. Zhou and J. Y. Lee, Periodic table for topological bands with non-Hermitian symmetries, *Phys. Rev. B* **99**, 235112 (2019).
- [8] E. J. Bergholtz, J. C. Budich, and F. K. Kunst, Exceptional topology of non-Hermitian systems, *Rev. Mod. Phys.* **93**, 015005 (2021).
- [9] Y. Ashida, Z. Gong, and M. Ueda, Non-Hermitian physics, *Adv. Phys.* **69**, 249 (2020).
- [10] N. Okuma, K. Kawabata, K. Shiozaki, and M. Sato, Topological Origin of Non-Hermitian Skin Effects, *Phys. Rev. Lett.* **124**, 086801 (2020).
- [11] D. S. Borgnia, A. J. Kruchkov, and R.-J. Slager, Non-Hermitian Boundary Modes and Topology, *Phys. Rev. Lett.* **124**, 056802 (2020).
- [12] N. Okuma and M. Sato, Quantum anomaly, non-Hermitian skin effects, and entanglement entropy in open systems, *Phys. Rev. B* **103**, 085428 (2021).
- [13] E. Edvardsson and E. Ardonne, Sensitivity of non-Hermitian systems, *Phys. Rev. B* **106**, 115107 (2022).
- [14] R. Verresen, N. G. Jones, and F. Pollmann, Topology and Edge Modes in Quantum Critical Chains, *Phys. Rev. Lett.* **120**, 057001 (2018).
- [15] R. Verresen, Topology and edge states survive quantum criticality between topological insulators, [arXiv:2003.05453](https://arxiv.org/abs/2003.05453).
- [16] R. Verresen, R. Thorngren, N. G. Jones, and F. Pollmann, Gapless Topological Phases and Symmetry-Enriched Quantum Criticality, *Phys. Rev. X* **11**, 041059 (2021).
- [17] O. Balabanov, D. Erkensten, and H. Johannesson, Topology of critical chiral phases: Multiband insulators and superconductors, *Phys. Rev. Res.* **3**, 043048 (2021).
- [18] O. Balabanov, C. Ortega-Taberner, and M. Hermanns, Quantization of topological indices in critical chains at low temperatures, *Phys. Rev. B* **106**, 045116 (2022).
- [19] C. Yin, H. Jiang, L. Li, R. Lü, and S. Chen, Geometrical meaning of winding number and its characterization of topological phases in one-dimensional chiral non-Hermitian systems, *Phys. Rev. A* **97**, 052115 (2018).
- [20] H. Jiang, C. Yang, and S. Chen, Topological invariants and phase diagrams for one-dimensional two-band non-Hermitian systems without chiral symmetry, *Phys. Rev. A* **98**, 052116 (2018).
- [21] S. Masuda and M. Nakamura, Relationship between the electronic polarization and the winding number in non-Hermitian systems, *J. Phys. Soc. Jpn.* **91**, 043701 (2022).
- [22] S. Sarkar, Quantization of geometric phase with integer and fractional topological characterization in a quantum Ising chain with long-range interaction, *Sci. Rep.* **8**, 5864 (2018).
- [23] I. Peschel, M. Kaulke, and Ö. Legeza, Density-matrix spectra for integrable models, *Ann. Phys. (Leipzig)* **511**, 153 (1999).
- [24] I. Peschel, Calculation of reduced density matrices from correlation functions, *J. Phys. A: Math. Gen.* **36**, L205 (2003).

- [25] I. Peschel and V. Eisler, The conceptual background of density-matrix renormalization, in *Computational Many-Particle Physics*, edited by H. Fehske, R. Schneider, and A. Weiße (Springer, Berlin, 2008), pp. 581–596.
- [26] L. Fidkowski, Entanglement Spectrum of Topological Insulators and Superconductors, *Phys. Rev. Lett.* **104**, 130502 (2010).
- [27] H. Yao and X.-L. Qi, Entanglement Entropy and Entanglement Spectrum of the Kitaev Model, *Phys. Rev. Lett.* **105**, 080501 (2010).
- [28] C. Ortega-Taberner and M. Hermanns, Relation of the entanglement spectrum to the bulk polarization, *Phys. Rev. B* **103**, 195132 (2021).
- [29] K. Monkman and J. Sirker, Entanglement properties of one-dimensional chiral topological insulators, [arXiv:2207.10558](https://arxiv.org/abs/2207.10558).
- [30] L. Herviou, J. H. Bardarson, and N. Regnault, Defining a bulk-edge correspondence for non-Hermitian Hamiltonians via singular-value decomposition, *Phys. Rev. A* **99**, 052118 (2019).
- [31] L. Herviou, N. Regnault, and J. H. Bardarson, Entanglement spectrum and symmetries in non-Hermitian fermionic non-interacting models, *SciPost Phys.* **7**, 069 (2019).
- [32] N. Hatano and D. R. Nelson, Localization Transitions in Non-Hermitian Quantum Mechanics, *Phys. Rev. Lett.* **77**, 570 (1996).
- [33] N. Hatano and D. R. Nelson, Vortex pinning and non-Hermitian quantum mechanics, *Phys. Rev. B* **56**, 8651 (1997).
- [34] N. Hatano and D. R. Nelson, Non-Hermitian delocalization and eigenfunctions, *Phys. Rev. B* **58**, 8384 (1998).
- [35] S. Yao and Z. Wang, Edge States and Topological Invariants of Non-Hermitian Systems, *Phys. Rev. Lett.* **121**, 086803 (2018).
- [36] P. Bonderson and C. Nayak, Quasi-topological phases of matter and topological protection, *Phys. Rev. B* **87**, 195451 (2013).
- [37] S. S. Pershoguba and V. M. Yakovenko, Shockley model description of surface states in topological insulators, *Phys. Rev. B* **86**, 075304 (2012).
- [38] R.-J. Slager, L. Rademaker, J. Zaanen, and L. Balents, Impurity-bound states and Green’s function zeros as local signatures of topology, *Phys. Rev. B* **92**, 085126 (2015).
- [39] H. Li and F. D. M. Haldane, Entanglement Spectrum as a Generalization of Entanglement Entropy: Identification of Topological Order in Non-Abelian Fractional Quantum Hall Effect States, *Phys. Rev. Lett.* **101**, 010504 (2008).
- [40] C. Ortega-Taberner, L. Rødland, and M. Hermanns, Polarization and entanglement spectrum in non-Hermitian systems, *Phys. Rev. B* **105**, 075103 (2022).
- [41] C.-T. Hsieh and P.-Y. Chang, Relating non-Hermitian and Hermitian quantum systems at criticality, [arXiv:2211.12525](https://arxiv.org/abs/2211.12525).
- [42] F. Schindler, K. Gu, B. Lian, and K. Kawabata, Hermitian bulk-Non-Hermitian boundary correspondence, [arXiv:2304.03742](https://arxiv.org/abs/2304.03742).
- [43] Y. Yi and Z. Yang, Non-Hermitian Skin Modes Induced by On-Site Dissipations and Chiral Tunneling Effect, *Phys. Rev. Lett.* **125**, 186802 (2020).